chemosensors

MDPI

Article

A Dinitrophenol-Based Colorimetric Chemosensor for Sequential Cu^{2+} and S^{2-} Detection

Hyejin Nam, Sungjin Moon *, Dongkyun Gil and Cheal Kim *

Department of Fine Chemistry and Renewable Energy Convergence, Seoul National University of Science and Technology (SNUT), Seoul 01098, Republic of Korea

* Correspondence: msjinjjang@naver.com (S.M.); chealkim@snut.ac.kr (C.K.)

Abstract: A dinitrophenol-based colorimetric chemosensor sequentially sensing Cu^{2+} and S^{2-}, **HDHT** ((*E*)-2-(2-(2-hydroxy-3,5-dinitrobenzylidene)hydrazineyl)-*N*,*N*,*N*-trimethyl-2-oxoethan-1-aminium), was designed and synthesized. The **HDHT** selectively detected Cu^{2+} through a color change of yellow to colorless. The calculated detection limit of the **HDHT** for Cu^{2+} was 6.4×10^{-2} μM. In the interference test, the **HDHT** was not considerably inhibited by various metal ions in its detection of Cu^{2+}. The chelation ratio of the **HDHT** to Cu^{2+} was determined as 1:1 by using a Job plot and ESI-MS experiment. In addition, the **HDHT**–Cu^{2+} complex showed that its color selectively returned to yellow only in the presence of S^{2-}. The detection limit of the **HDHT**–Cu^{2+} complex for S^{2-} was calculated to be 1.2×10^{-1} μM. In the inhibition experiment for S^{2-}, the **HDHT**–Cu^{2+} complex did not significantly interfere with other anions. In the real water-sample test, the detection performance of the **HDHT** for Cu^{2+} and S^{2-} was successfully examined. The detection features of **HDHT** for Cu^{2+} and the **HDHT**–Cu^{2+} for S^{2-} were suggested by the Job plot, UV–Vis, ESI-MS, FT-IR spectroscopy, and DFT calculations.

Keywords: dinitrophenol; colorimetric chemosensor; Cu^{2+}; S^{2-}; DFT calculation

Citation: Nam, H.; Moon, S.; Gil, D.; Kim, C. A Dinitrophenol-Based Colorimetric Chemosensor for Sequential Cu^{2+} and S^{2-} Detection. *Chemosensors* **2023**, *11*, 143. https://doi.org/10.3390/chemosensors11020143

Academic Editors: Eduardo Torres and Ilaria Palchetti

Received: 3 January 2023
Revised: 9 February 2023
Accepted: 14 February 2023
Published: 15 February 2023

1. Introduction

Various detection methods for metal ions and anions are used, such as atomic absorption–emission spectrometry, surface-plasmon resonance detectors, the electrochemical method, inductively coupled plasma detectors and the fluorescence technique [1,2]. However, these methods need technical operators, costly equipment, and, in some cases, significant time and cost [3–6]. Compared to the methods above, the colorimetric chemosensing method is not only simple and fast but is also used for on-site tests [7–10].

Among the diverse trace metal ions, Cu^{2+} performs a significant role in living organisms [11–13]. However, the excessively accumulation of Cu^{2+} can result in significant damage to the nervous system, which induces Alzheimer's, Menkes, and Wilson's diseases [14–18]. Due to the hazardous effect of Cu^{2+}, the Environmental Protection Agency (EPA) limits the acceptable Cu^{2+} concentration in drinking water to 20 μM [19]. Thus, the presence and quantities of Cu^{2+} should be continuously monitored [20]. Sulfide (S^{2-}) is reported to perform an important role in biological systems, such as apoptosis, vasodilation, infections caused by inflammation, angiogenesis, and neurological disorders [21,22]. However, sulfide a high levels is known as a toxic and hazardous contaminant material [23–25]. The guideline of S^{2-} in freshwater suggested by the WHO is 14.8 μM [26]. Nevertheless, sulfide is widely and easily detected in various environments, such as industries, pesticides, automobiles, bleaching powder, and even the natural environment [27–29]. Therefore, there is a need to develop methods to detect sulfide easily, quickly, and conveniently in both environmental and biological systems [30]. Interestingly, the chemosensors detecting Cu^{2+} could be used to detect S^{2-} due to the formation of the stable CuS compound

(K_{sp} = 6.3 × 10^{-36}) [31]. Therefore, if a sensor detecting Cu^{2+} were to be developed, it could be used as a sensor for detecting S^{2-}.

Several colorimetric chemosensors have been developed for sequential Cu^{2+} and S^{2-} detection, to date (Table S1). These chemosensors have diverse chromophores, such as benzo[c][1,2,5]thiadiazole [1], benzo[d]thiazole [21], and fluorescein [32] moieties, as well as long conjugation systems [21,31,33], to induce dramatic color changes. In addition, the functional groups inducing the intramolecular-charge transfer (ICT) properties were applied to the design of colorimetric chemosensors [30,31,34,35]. However, many of them have difficulty in efficiently detecting Cu^{2+} and S^{2-} in water due to their low solubility [1,36,37]. The poor water solubility of these chemosensors is a major drawback for their application to real environmental samples. Therefore, designing chemosensors to probe Cu^{2+} and S^{2-} in water is a significant challenge.

From this point of view, we utilized the dinitrophenol and (hydrazinocarbonylmethyl)trimethylammonium chloride (Girard's Reagent T) moieties to develop a highly water-soluble chemosensor based on ICT. A strong electron-withdrawing nitro group (-NO_2) acts as an electron acceptor in electron-push—pull design, and this property of the nitro group could be a useful chromophore [38–40]. Therefore, the dinitrophenol with two nitro groups was selected as a chromophore group. In addition, the nitro-phenol group may provide a chelating site for metal ions. Next, a very water-soluble molecule, Girard's Reagent T, was selected as another functional group to increase the solubility of a designed chemosensor in water [41–43]. These characteristics of the compounds led us to expect that a molecule produced from the combination of the dinitrophenol and Girard's reagent T could be used as a chemosensor to detect metal ions, such as Cu^{2+}, in water.

In this paper, we present a newly synthesized dinitrophenol-based chemosensor, **HDHT**. The chemosensor **HDHT** could sense Cu^{2+} with a color change of yellow to colorless in near-perfect water. Moreover, the **HDHT**-Cu^{2+} could analyze S^{2-} through the demetallation of Cu^{2+} from the **HDHT**-Cu^{2+} with a color change of colorless to yellow. Importantly, the detection limits (6.4 × 10^{-2} μM and 1.2 × 10^{-1} μM) of the **HDHT** for Cu^{2+} and S^{2-} were below the guidelines (20 μM and 14.8 μM) suggested by the EPA and the WHO, respectively. The binding features of the **HDHT** to the Cu^{2+} and the **HDHT**-Cu^{2+} to the S^{2-} were explained by UV–Visible titrations, Job plot, ESI-MS, FT-IR spectroscopy, and density-functional-theory calculations.

2. Experimental Section

2.1. Materials and Instrumentations

The (Hydrazinocarbonylmethyl)trimethylammonium chloride (Girard's Reagent T) and 3,5-dinitrosalicyladehyde were obtained from Alfa Aesar and TCI. The Bis-tris buffer was acquired from Sigma Aldrich. Buffer solutions of pH 1–13 were obtained from Samchun in Korea. Varian and Perkin Elmer spectrometers were used to obtain ^{1}H & ^{13}C NMR and absorption spectra. Varian 640-IR and Thermo MAX instrument were used to obtain FT-IR and ESI-MS spectra.

*2.2. Synthesis of Chemosensor **HDHT** ((E)-2-(2-(2-Hydroxy-3,5-dinitrobenzylidene)hydrazineyl)-N,N,N-trimethyl-2-oxoethan-1-aminium) Chloride)*

The **HDHT** was synthesized by the imine-formation reaction of Girard's Reagent T and 3,5-dinitrosalicyladehyde. Girard's reagent T (1.71 × 10^2 mg, 1 mmol) was added to ethanol 20 mL. Subsequently, 3,5-Dinitrosalicyladehyde (2.38 × 10^2 mg, 1.1 mmol) was added to the solution. The mixture was stirred for 3 h at 22 °C. The powder filtered was washed with ethanol. After drying in a vacuum, an orange powder was obtained. Yield: 332.9 mg (92 %). ^{1}H NMR (400 MHz, DMF-d_7): δ = 12.15 (s, 0.55 H), 9.02 (s, 0.56 H), 8.90 (d, 0.56 H), 8.86 (d, 0.56 H), 8.75 (d, 0.44 H), 8.68 (s, 0.44 H), 8.58 (d, 0.44 H), 5.10 (s, 0.88 H), 4.75 (s, 1.12 H), 3.60 (s, 3.96 H), 3.58(s, 5.06 H); ^{13}C NMR (175 MHz, DMSO-d_6): δ = 165.47, 161.72, 160.45, 159.32, 145.53, 141.27, 137.83, 137.66, 135.70, 133.08, 127.08, 126.79, 124.30,

124.26, 123.68, 123.16, 63.10, 62.28, 53.61, 53.35. ESI-MS: m/z calcd for ([**HDHT** − H^+])$^-$, 360.07; found, 359.69 and ([**HDHT** + MeOH − H^+])$^-$, 392.10; found, 391.89.

2.3. UV–Vis Titration

The **HDHT** (3.7 mg, 1×10^{-5} mol) was dissolved in DMSO (1 mL) to make a 10-millimolar **HDHT** stock solution. To make 20 mM of a Cu^{2+} stock solution, $Cu(NO_3)_2$ (23.7 mg, 1×10^{-1} mmol) was dissolved in 5.0×10^{-3} L of bis-tris buffer. The **HDHT** solution (30 μM) was produced by diluting 9 μL of 10 mM **HDHT** into a 2991-microliter buffer. Next, 0–58.5 μL of the Cu^{2+} stock (2×10^{-3} M) was added to 30 μM of the prepared **HDHT** solution. The UV–Vis titration was performed in 5 s.

For S^{2-}, 3 mL of a 10-micromolar **HDHT**-Cu^{2+} stock was produced by diluting 1 mL of an **HDHT** stock (30 mM) and 1.95 mL of a $Cu(NO_3)_2$ stock (2×10^{-2} M) to 0.05 mL buffer. In total, 9 μL of the prepared **HDHT**-Cu^{2+} stock (1×10^{-2} M) was transferred to 2991 μL of the buffer. Next, 0–15.3 μL of Na_2S stock (0.01 M) was added to 30 μM of complex stock solution. The UV–Vis titration was performed in 5 s.

2.4. Job-Plot Analysis

To prepare 1 mL of a 10-micromolar **HDHT** stock solution, **HDHT** (1×10^{-2} mmol, 3.7×10^{-3} g) was dissolved in 1000 μL of DMSO. A Cu^{2+} solution (10 mM) with its nitrate salt was acquired in a 1000 = microliter buffer solution. In total, 3–27 μL of the **HDHT** stock were transferred to several quartzes. Furthermore, 3–27 μL of the Cu^{2+} solution were added to diluted **HDHT**. Each quartz was filled with bis-tris buffer to create a 3000-microliter solution with a total concentration of 0.1 mM. Next, UV–Vis spectra were collected.

2.5. UV–Vis Inhibition Tests

The **HDHT** (3.7 mg, 1×10^{-5} mol) was dissolved in DMSO (1000 μL). The various metal-cation stocks (Ni^{2+}, Cu^{2+}, Ga^{3+}, Fe^{3+}, In^{3+}, Hg^{2+}, Zn^{2+}, Na^+, Cd^{2+}, Fe^{3+}, Mg^{2+}, Ca^{2+}, Cr^{3+}, Ag^+, Pb^{2+}, K^+, Mn^{2+}, Co^{2+}, and Al^{3+}) were prepared by dissolving 1×10^{-4} mol of each metal cation in 5×10^{-3} L of buffer, respectively. In total, 5.9×10^{-6} L of each metal ion (2×10^{-2} M) and Cu^{2+} (20 mM) were added into 3×10^{-3} L buffer. Next, 9×10^{-6} L of the **HDHT** stock (10 mM) were added to the solution. After mixing the mixture for 5 s, an inhibition test was performed.

For S^{2-}, the **HDHT** (1×10^{-5} mol, 3.7 mg) was dissolved in 1 mL DMSO, and $Cu(NO_3)_2$ (23.7 mg, 1×10^{-4} mmol) was dissolved in 5.0 mL of buffer. Next, 100 μL of the **HDHT** stock and 65 μL of the Cu^{2+} stock were diluted by 835 μL of buffer to make 1 mM of **HDHT**-Cu^{2+} complex solution. Stock solutions containing 100 mM of Et_4NF, Et_4NBr, Et_4NCl, Et_4NI, Et_4NCN, $Bu_4N(OAc)$, $Bu_4N(H_2PO_4)$, $Bu_4N(SCN)$, $Bu_4N(BzO)$, Na_2S, $Bu_4N(N_3)$, and $NaNO_2$ were prepared by dissolving 5×10^{-4} mol of each anion in 5.0 mL of buffer, respectively. Next, 1.5 μL of each anion (100 mM) and S^{2-} (100 mM) were added into a 2.904-milliliter bis-tris buffer. A total of 90 μL of the **HDHT**-Cu^{2+} (1 mM) was transferred to the solution. An inhibition test was performed in 5 s.

2.6. pH Test

The **HDHT** (3.7 mg, 1×10^{-2} mmol) was dissolved in DMSO (1.0 mL). To prepare 3×10^{-2} mM 9 μL of the **HDHT** stock, (1 mM) was transferred to 2994 μL of each pH buffer. The $Cu(NO_3)_2$ (2.37×10^{-2} g, 1×10^{-1} mmol) was dissolved in 5 mL of buffer. Next, 6.5×10^{-2} mL of the Cu^{2+} stock was transferred to the pH buffer solution. A pH test was performed in 5 s.

For S^{2-}, **HDHT** (3.7×10^{-3} g, 1×10^{-2} mmol) was dissolved in DMSO (1×10^{-3} L), and 23.7mg (0.1 mmol) of $Cu(NO_3)_2$ was liquefied in 5.0-milliliter bis-tris buffer. Next, 100 μL of the **HDHT** stock and 65 μL of the Cu^{2+} stock were diluted by 835 μL of buffer to prepare 1 mM of **HDHT**–Cu^{2+}-complex solution. A S^{2-} stock (100 mM) was prepared by dissolving Na_2S (0.5 mmol, 1.22×10^2 mg) in 5 mL of the bis-tris buffer. A total of 90 μL of the **HDHT**-Cu^{2+} stock (1×10^{-3} M) was transferred to 2.91×10^{-3} L of each pH solution

to make 3×10^{-2} mM. Next, 1.5×10^{-3} mL of the Na_2S stock (0.1 M) was added to each pH solution. A pH test was performed in 5 s.

2.7. Real-Water-Sample Detection

The drinking and tap water for the real-water-sample experiment was obtained in our laboratory. A 10-millimolar stock of **HDHT** was created by dissolving **HDHT** (3.7×10^{-3} g, 1×10^{-2} mmol) in DMSO (1000 µL). The $Cu(NO_3)_2$ (23.7 mg, 100 µmol) was dissolved in 5 mL of buffer (10 mM, pH 7.00) to prepare a Cu^{2+} stock (20 mM). In total, 9×10^{-3} mL of the 10-micromolar **HDHT** stock were added to 2.997 mL of drinking or tap water, which contained Cu^{2+} (9.0 µM). The UV–Vis spectra were taken in 5 s.

For sulfide, 10 mM of a **HDHT** (3.7×10^{-3} g, 1×10^{-2} mmol) stock dissolved in DMSO (1000 µL), and 20 mM of a $Cu(NO_3)_2$ (23.7 mg, 0.1 mmol) stock dissolved in 5.0 mL of buffer were prepared. Next, to make 1 mM of **HDHT**-Cu^{2+} stock, 100 µL of the **HDHT** stock and 65 µL of the Cu^{2+} stock were diluted in 835 µL of the buffer. A total of 90 µL of this diluted **HDHT**-Cu^{2+} (1×10^{-3} M) was added to 2940 µL of a sample solution containing S^{2-} (4.5 µM). The UV–Vis spectra were taken in 5 s.

2.8. Theoretical Calculations

To investigate the detection mechanism of the **HDHT** for Cu^{2+}, the Gaussian16 program was used for calculations based on B3LYP density functional [44–46]. Basis sets of 6–31G (d,p) [47,48] and Lanl2DZ [49] were employed for calculations of elements and Cu^{2+}. Neither the **HDHT**-Na nor the **HDHT**-Cu^{2+} form exhibited imaginary frequencies, resulting in local minima. The effect of water as solvent was considered by employing IEFPCM [50]. With the optimized patterns of **HDHT** and **HDHT**-Cu^{2+}, 20 of the lowest singlet states were calculated with TD-DFT method to study their transition states.

3. Results and Discussion

*3.1. Synthesis and Structural Characteristics of **HDHT***

A novel nitrophenol-based chemosensor **HDHT** was produced via the condensation reaction of Girard's Reagent T and 3,5-dinitrosalicyladehyde (Scheme 1). The **HDHT** was verified with ^{1}H NMR, ^{13}C NMR, and ESI-MS (Figures S1–S3). The **HDHT** showed two different structures with rotational isomers (*syn* and *anti*; Figures S1 and S2). The rotational isomers appear with the rotation of the C–N bond in amide [51,52]. The DFT calculations showed that the optimized *anti* isomer was slightly more stable than the *syn* isomer, by 2.95 kcal/mol (Figure S4). The calculation results were matched with the ^{1}H NMR spectrum of the **HDHT**, resulting in a ratio of 44:56 (*syn*:*anti*) (Figure S1).

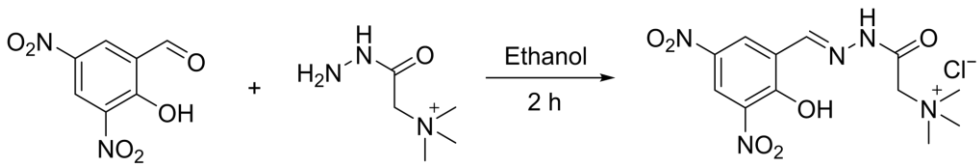

Scheme 1. Synthesis of **HDHT**.

*3.2. Application of **HDHT** with Cu^{2+}*

The colorimetric detection using **HDHT** was examined with various metal ions in a bis-tris buffer (pH = 7.0, Figure 1). As diverse cations were transferred to the **HDHT**, only the Cu^{2+} caused a remarkable decrease at 430 nm in the UV–Vis spectra (Figure 1a) and displayed a color change of yellow to colorless (Figure 1b). The zinc and cobalt ions showed a slight decrease in absorbance, and ferrous and ferric ions revealed their own pale orange color. These results demonstrated that **HDHT** can detect only Cu^{2+} with a color variation.

(**a**)

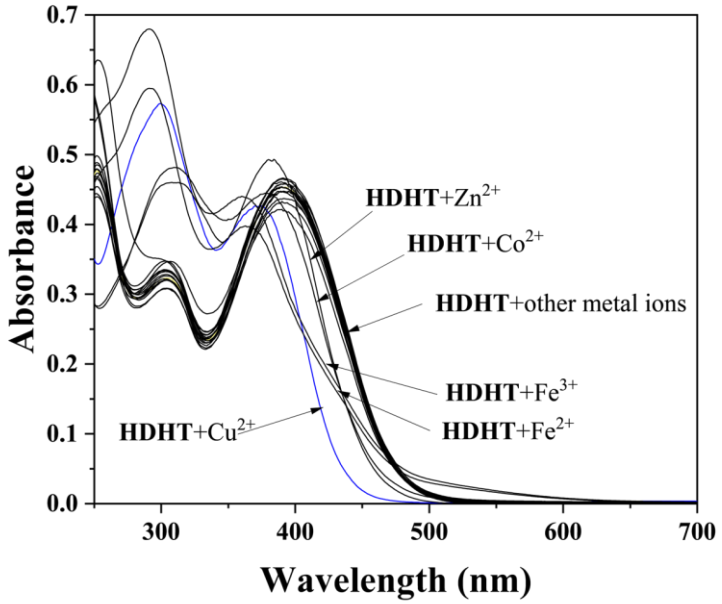

(**b**)

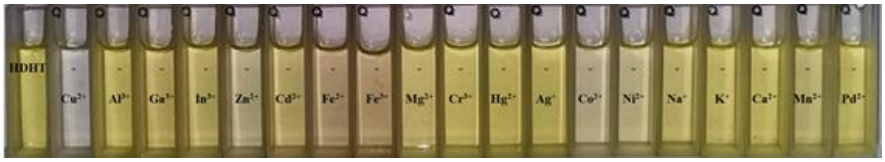

Figure 1. (**a**) Absorbance spectra of **HDHT** (30 μM) with metal ions (39 μM). (**b**) Photograph of color changes of **HDHT** (30 μM) with metal ions (39 μM).

The UV–Vis titration was performed to study the chelating mode of the **HDHT** with Cu^{2+} (Figure 2). The free **HDHT** displayed two main absorbance bands at 305 and 394 nm (molar extinction coefficient: 11,183 $M^{-1}cm^{-1}$ and 15,623 $M^{-1}cm^{-1}$, respectively), indicating ICT transition. With the increment of the Cu^{2+}, the absorbance at 304 nm increased and those at 430 nm and 250 nm decreased. This hypsochromic shift may have been caused by the Cu^{2+} interfering with the ICT process. The isosbestic point was checked at 373 nm, implying that the **HDHT** and Cu^{2+} generated the one chemical species. A Job-plot experiment was carried out to determine the complexation ratio of the **HDHT** with the Cu^{2+} (Figure 3). When the ratio of ([**HDHT**]/[**HDHT**] + [Cu^{2+}]) was 0.5, the absorbance at 430 nm reached its maximum. This result indicated that the **HDHT** chelated with the Cu^{2+} in a 1:1 ratio. To support the binding ratio of the **HDHT** with the Cu^{2+}, an ESI-MS analysis was performed (Figure S5). The peak of 484.44 (m/Z) was assignable to be [**HDHT** + Cu^{2+} − $2H^+$ + NO_3^-]$^-$ (calcd. 483.98). Based on the calibration curve with the Cu^{2+}, the binding constant of the **HDHT** with the Cu^{2+} was calculated as 1.97×10^4 M^{-1} by the Benesi–Hildebrand equation (Figure S6). The calculated binding constant was within the previously reported range (10^3–10^{12}) for Cu^{2+} sensors [30,31,35,37,53]. The detection limit for Cu^{2+} was calculated to be 6.4×10^{-2} μM in the range of 0–7.5 μM using the definition by IUPAC ($C_{DL} = 3\sigma/k$; Figure 4). Importantly, the **HDHT** showed the lowest detection limit for Cu^{2+} among the color-changeable chemosensors sequentially operating for Cu^{2+} and S^{2-} in near-perfect water (Table S1). To study the interaction of the **HDHT** with the Cu^{2+}, a FT-IR analysis was carried out (Figure S7). The C=O bond of the carbonyl group assigned to the peak at 1712 cm^{-1} was moved to 1619 cm^{-1} [54,55], and the peak at 1609 cm^{-1} specified to the C=N bond was shifted to 1596 cm^{-1} [56]. The N-H and O-H with hydrogen-bonding character were observed in broad conformations. These results suggested that the Cu^{2+} coordinated with the hydroxyl, the imine, and the carbonyl groups.

With the FT-IR analysis, the ESI-MS, and the Job plot, the probable features of **HDHT** with Cu^{2+} was proposed (Scheme 2).

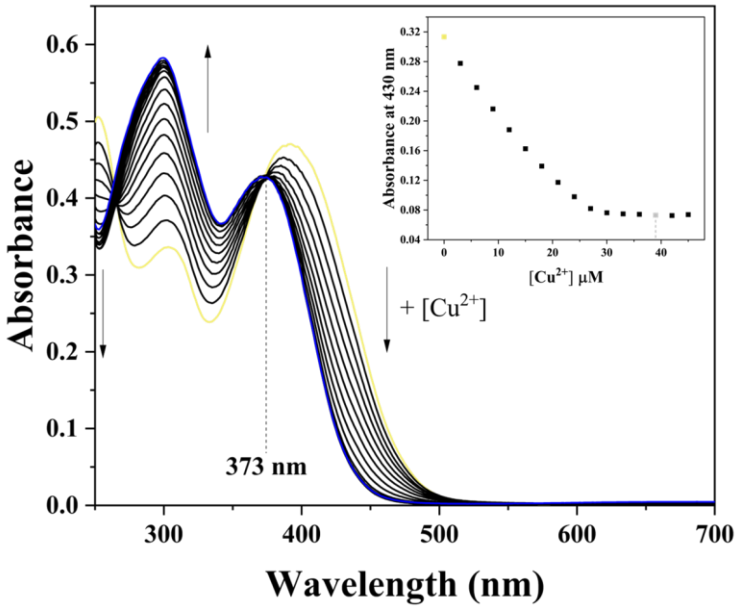

Figure 2. Absorbance spectra of **HDHT** (30 μM) with different concentrations of Cu^{2+} (0–45 μM) (yellow line: **HDHT**; blue line: **HDHT** + 39 μM Cu^{2+}).

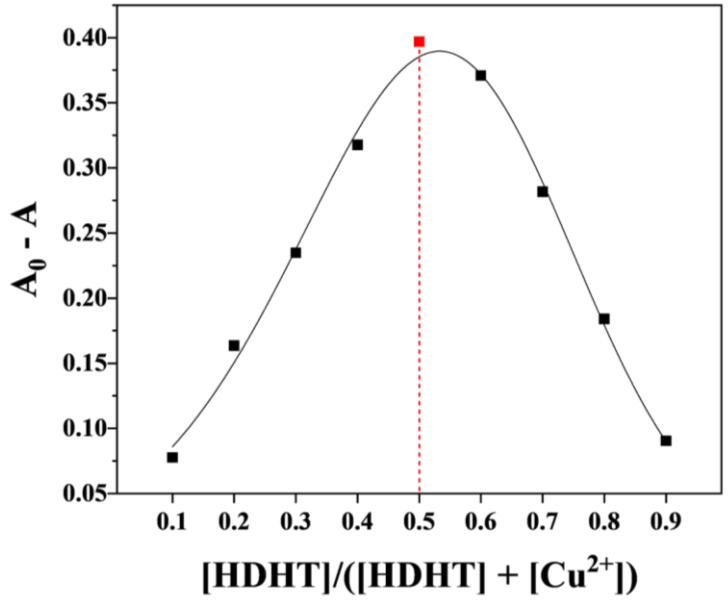

Figure 3. Job-plot analysis for determining the stoichiometry of **HDHT** and Cu^{2+} at 430 nm (red line: ([**HDHT**]/[**HDHT**] + [Cu^{2+}]) = 0.5).

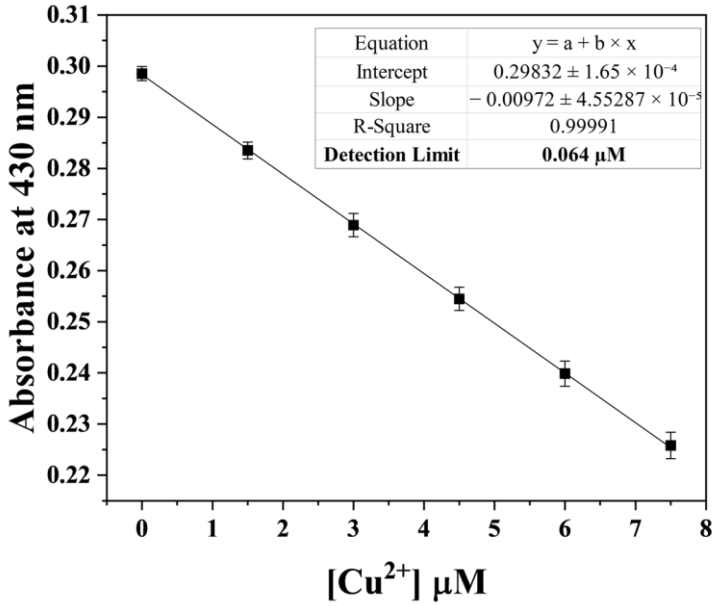

Figure 4. Calibration curve for Cu^{2+} analysis using **HDHT** plotted against absorbance at 430 nm (n = 3).

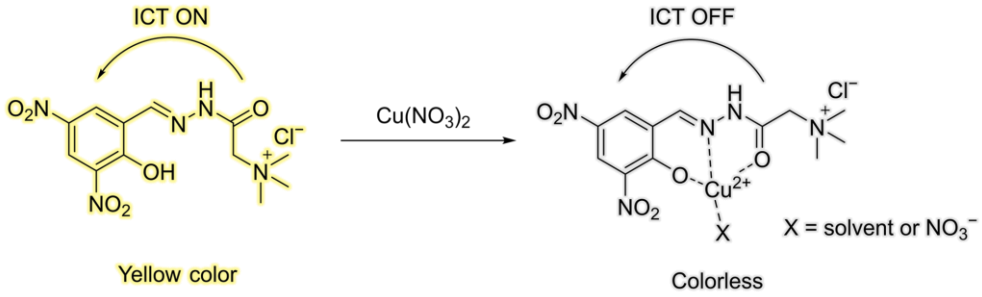

Scheme 2. Proposed chelating mode of **HDHT** with Cu^{2+}.

The competition experiment was undertaken to study the preferable selectivity of **HDHT** for Cu^{2+} in a competitive environment (Figure 5). None of the metal ions tested showed any competitive effect on the Cu^{2+} (Figure 5a). To the naked eye, except for the Cu^{2+}, none of the metal ions showed a color change when added to the **HDHT** (Figure 5b). In the absence of any interference from other metal ions, **HDHT** can be used for the detection of Cu^{2+}. The pH test was performed to examine the dependence of the sensing ability of the **HDHT** on the pH (Figure S8). The experiment results revealed that the **HDHT** worked suitably to detect Cu^{2+} in a pH range of 5–11. These results signified that the **HDHT** could efficiently detect the Cu^{2+} in the physiological pH range of 7.0–8.4, as well as in basic and acidic conditions. The recovery test was accomplished to study whether **HDHT** could quantify Cu^{2+} in real water samples, such as tap and drinking water (Table 1). The percentage of recovery and relative standard deviation (R.S.D.) indicated appropriate results, demonstrating that **HDHT** can properly determine Cu^{2+} in real water samples. Moreover, based on these results, **HDHT** can be applied to determine Cu^{2+} in a stream containing a variety of cations around an industrial complex.

(**a**)

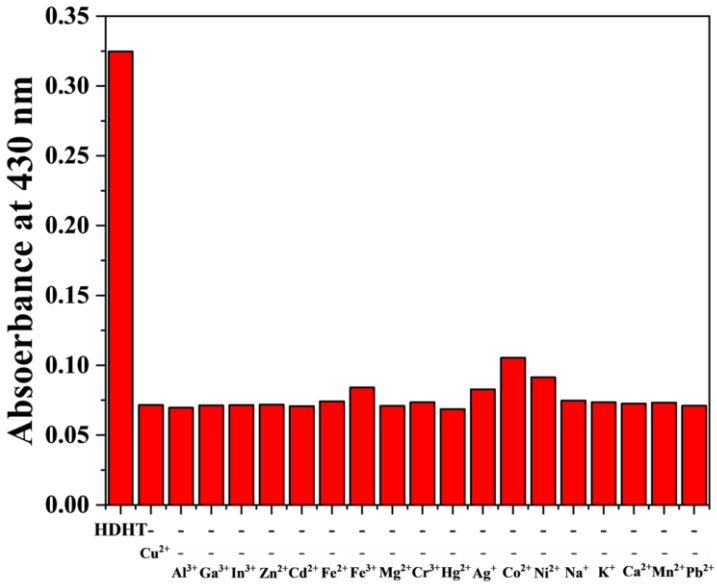

(**b**)

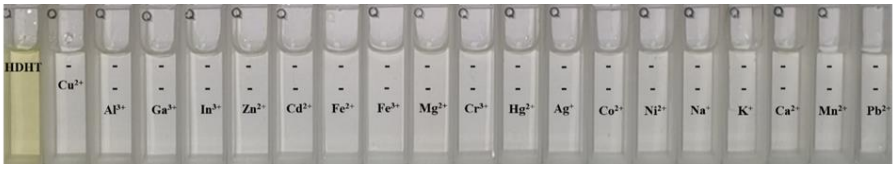

Figure 5. Inhibition test. (**a**) Absorbance of **HDHT** (30 μM) at 430 nm in the presence of Cu^{2+} (39 μM) and other metal ions (39 μM). (**b**) Photograph of color changes of 30 μM **HDHT** solution in the presence of Cu^{2+} (39 μM) and other ions (39 μM).

Table 1. Recovery-test results for Cu^{2+} in real water samples *.

Sample	Cu^{2+} Added (μM)	Cu^{2+} Added (μM)	Recovery (%)	R.S.D. (*n* = 3) (%)
Drinking water	0	0	-	-
	9.00	9.17	101.89	3.71
Tap water	0	0	-	-
	9.00	8.81	97.89	2.29

* Conditions: **HDHT** = 30 μM in buffer.

3.3. Theoretical Study

In order to investigate the interaction between the **HDHT** and the Cu^{2+}, a number of calculations were performed. The calculations of the **HDHT**–Cu^{2+} were based on the 1:1 chelation of **HDHT** and Cu^{2+}, which was proposed by the ESI-MS and the Job plot. As shown in Figure S9, as a tridentate ligand, **HDHT** chelates Cu^{2+} using hydroxyl oxygen, imine nitrogen, and carbonyl oxygen. The **HDHT**–Cu^{2+} complex showed a square planar structure with one NO_3^-. With the optimized features, the TD-DFT calculations were performed to check the electronic transitions of the **HDHT** and the **HDHT**–Cu^{2+}. For the **HDHT**, excited state 1 (409.32 nm) was regarded as the HOMO → LUMO transition, showing an ICT property (Figures S10 and S11). Its molecular orbitals indicated the shift of the electron cloud from the amide group to the 3,5-dinitrophenol moiety. The ICT character caused the yellow color of the **HDHT**. For the **HDHT**–Cu^{2+}, excited state 16 (367.70 nm) consisted of HOMO → LUMO (alpha) and HOMO → LUMO+1 (beta), which showed $\pi \rightarrow \pi^*$ characters (Figures S11 and S12). As shown in Figure S11, the energy-gap change in the **HDHT** (3.560 eV) and **HDHT**-Cu^{2+} (3.970 eV (alpha) and 3.930 eV (beta)) was clearly

consistent with the hypsochromic shift in the experimental results. These results showed that the ICT process was inhibited due to the formation of a coordination bond between the **HDHT** and the Cu^{2+}. Thus, the reason for the color change of the **HDHT** from yellow to colorless with the addition of Cu^{2+} can be explained by the repression of the ICT process. With the Job plot, ESI-MS, FT-IR, and DFT calculations, we suggested the mechanism of the colorimetric sensing of Cu^{2+} by **HDHT** (Scheme 2).

*3.4. Application of **HDH**–Cu^{2+} Complex for S^{2-} Sensing*

For the **HDHT**–Cu^{2+} complex, the selectivity experiment was performed with various anions. When the anions were added to the complex solution, only S^{2-} showed a significant increase in absorbance at 430 nm and a color change of colorless to yellow (Figure 6). These results suggested that the **HDHT**–Cu^{2+} had selectivity for S^{2-}. The UV–Vis titration was performed for S^{2-} (Figure 7). The absorbance of 300 nm decreased and that of 430 nm increased when S^{2-} was added. The sensing mechanism of the **HDHT**–Cu^{2+} for S^{2-} was further investigated by ESI-MS. As shown in Figure S13, the peak of 435.86 (m/Z) was assigned to [**HDHT** - H^+ + Na^+ + $3H_2O$]$^-$ (calcd. 436.09), which suggests that S^{2-} binds and removes Cu^{2+} from the **HDHT**–Cu^{2+} complex. With the results of the experiment data, the plausible detection mechanism of **HDHT**–Cu^{2+} for S^{2-} was proposed (Scheme 3). The obtained detection limit was 0.12 μM in the scope of 0 μM to 8 μM of sulfide (Figure 8). Remarkably, the **HDHT** showed the lowest detection limit for S^{2-} among the color-variable chemosensors sequentially analyzing for Cu^{2+} and S^{2-} in ultrapure water (Table S1). The interference study was performed to investigate whether the presence of other anions affects the detection of S^{2-}. In the inhibition test, the **HDHT**-Cu^{2+} did not show significant interference in detecting S^{2-} against other anions (Figure 9a). Observations using the naked eye revealed no interference with the detection of S^{2-} in the presence of other anions (Figure 9b). To determine the effect of pH on S^{2-} detection by the **HDHT**–Cu^{2+}, the pH test was performed (Figure S14). At pH 3–12, it was confirmed that the **HDHT**–Cu^{2+} worked well, without any problems. This observation demonstrated that the **HDHT** can effectively detect not only Cu^{2+} but also S^{2-} through sequential detection over a wide range of pH. The recovery test was conducted to examine whether the **HDHT**–Cu^{2+} could detect S^{2-} in a real-water sample, such as drinking water (Table 2). The displayed result suggested that **HDHT**–Cu^{2+} can appropriately detect S^{2-} in a real environment.

(**a**)

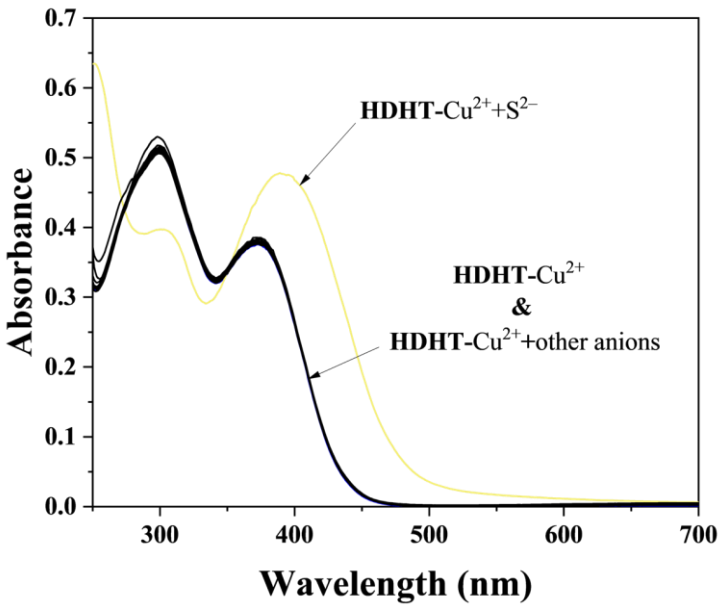

Figure 6. *Cont.*

(**b**)

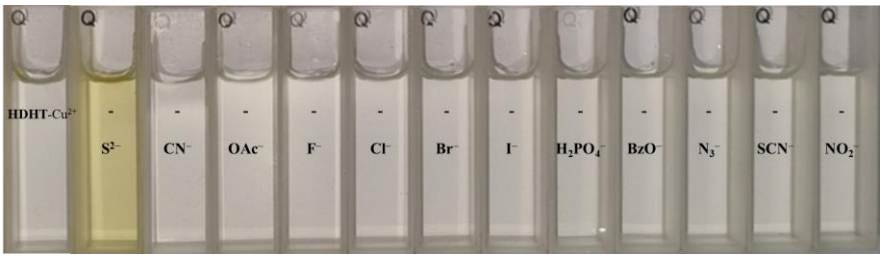

Figure 6. (**a**) Absorbance spectra of **HDHT**–Cu^{2+} (30 μM) with a variety of anions (51 μM). (**b**) Photograph of color changes of **HDHT**–Cu^{2+} (30 μM) with a variety of anions (51 μM).

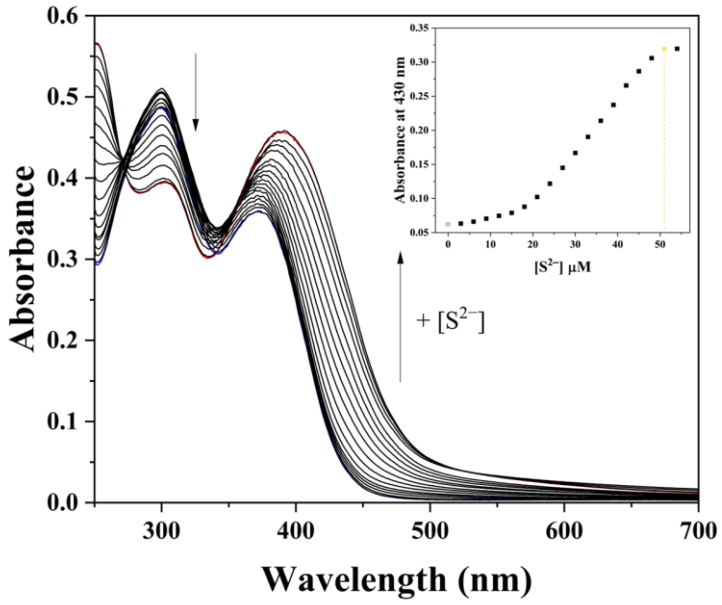

Figure 7. Absorbance spectra of **HDHT**–Cu^{2+} complex (30 μM) with different concentrations of S^{2-} (0–54 μM) (blue line: **HDHT**–Cu^{2+}; red line: **HDHT**–Cu^{2+} + 51 μM S^{2-}).

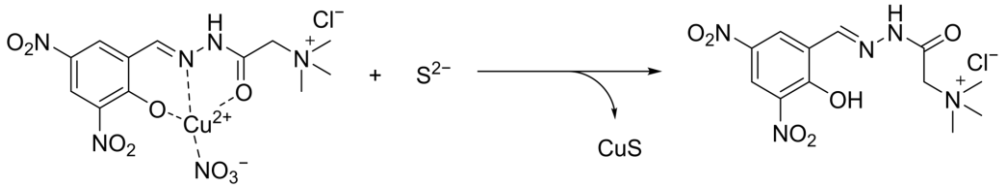

Scheme 3. Proposed detection feature of **HDHT**–Cu^{2+} with S^{2-}.

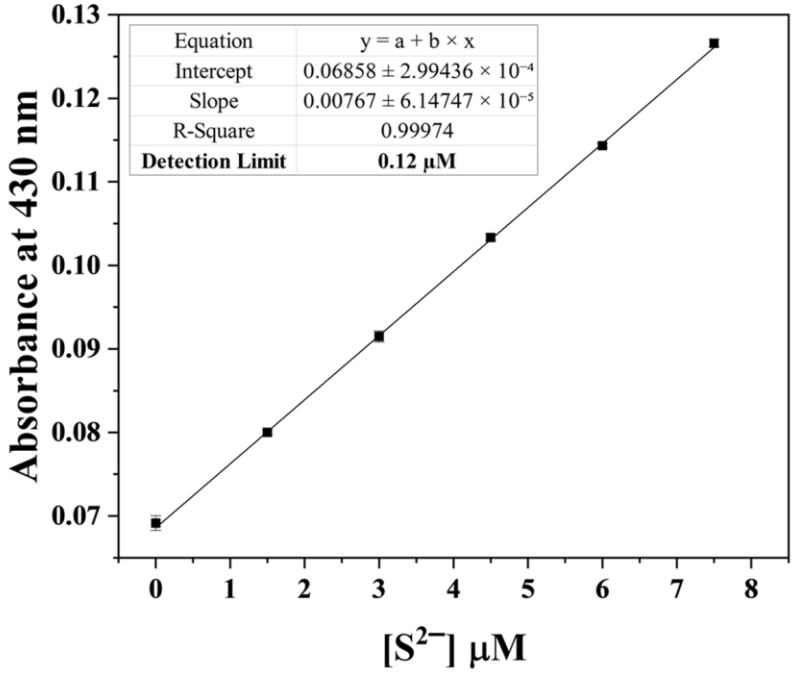

Figure 8. Calibration curve for S^{2-} analysis using **HDHT**–Cu^{2+} plotted against absorbance at 430 nm (n = 3).

(**a**)

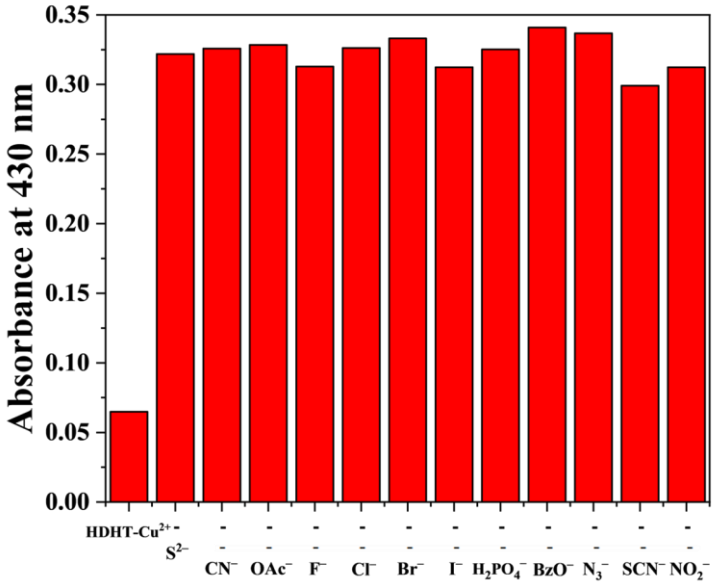

(**b**)

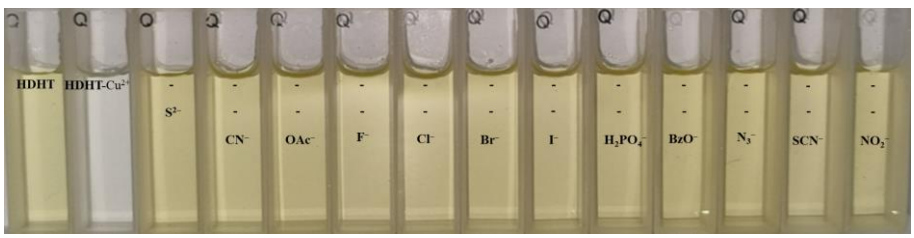

Figure 9. Inhibition test. (**a**) Absorbance of **HDHT**–Cu^{2+} complex (30 μM) at 430 nm in the presence of S^{2-} (51 μM) and other anions (51 μM). (**b**) Photograph of color changes of 30 μM **HDHT**-Cu^{2+} solution in the presence of S^{2-} (51 μM) and other anions (51 μM).

Table 2. Recovery-test results for S^{2-} in the real-water sample *.

Sample	Na_2S Added (μM)	Na_2S Added (μM)	Recovery (%)	R.S.D. (*n* = 3) (%)
Drinking water	0	0	-	-
	4.5	4.38	97.33	0.48

* Conditions: [**HDHT**–Cu^{2+}] = 30 μM in buffer.

4. Conclusions

We addressed a dinitrophenol-based sequential colorimetric chemosensor, **HDHT**, which can clearly probe Cu^{2+} and S^{2-}. With a Job plot and ESI-MS, the structure of the association of **HDHT** with Cu^{2+} was found to be a 1:1 ratio. The detection limit and binding constant of **HDHT** to Cu^{2+} were 6.4×10^{-2} μM and 1.97×10^{4} M^{-1}, respectively. The detection limit for Cu^{2+} was clearly below the EPA standard (20 μM). Importantly, the **HDHT** was able to detect the Cu^{2+} under weak-acid-to-strong-base conditions and quantify Cu^{2+} in real environments, such as tap and drinking water. Meanwhile, the **HDHT**–Cu^{2+} showed a sequential detection for S^{2-}. The detection limit of the **HDHT**–Cu^{2+} to the S^{2-} was 1.2×10^{-1} μM. This detection limit was lower than the WHO freshwater guideline (14.8 μM) for S^{2-}. It was noteworthy that the **HDHT**–Cu^{2+} was able to quantify S^{2-} from pH 3 to pH 12 and detect S^{2-} in real water. Most importantly, the **HDHT** showed the lowest detection limits for Cu^{2+} and S^{2-} among color-changeable chemosensors sequentially operating for Cu^{2+} and S^{2-} in near-perfect water. The sensing features of the **HDHT** for Cu^{2+} and S^{2-} were described by a Job plot, ESI-MS, UV-vis, FT-IR, and calculations. Hence, we expect that these findings could provide inspiration for the development of a novel color-changeable chemosensor for sequentially detecting Cu^{2+} and S^{2-} in water.

Supplementary Materials: The following supporting information can be downloaded at: https://www.mdpi.com/article/10.3390/chemosensors11020143/s1. Table S1. Examples of chemosensors for sequential detection of Cu^{2+} and S^{2-} through color variation in aqueous solution [57]; Figure S1. ^{1}H NMR spectrum of **HDHT**; Figure S2. ^{13}C NMR spectrum of **HDHT**; Figure S3. Negative-ion ESI-MS spectra of **HDHT** (100 μM); Figure S4. Gibbs free energy (ΔG°_{f}) calculation for optimized isomers of **HDHT**; Figure S5. Negative-ion ESI-MS spectra of **HDHT** (100 μM) with Cu^{2+} (100 μM); Figure S6. The binding constant of **HDHT** (30 μM) with Cu^{2+} when using the Benesi–Hildebrand method. The absorbance spectrum at 430 nm is measured by the increasing equivalent of Cu^{2+}; Figure S7. FT-IR spectra of **HDHT** (black line) and **HDHT**–Cu^{2+} (red line); Figure S8. The pH-stability test. (a) UV–Vis absorbance at 430 nm of **HDHT** (30 μM) and **HDHT**–Cu^{2+} (30 μM) in buffer solution from pH 1 to pH 13. (b) Color change of **HDHT** (30 μM) and **HDHT**–Cu^{2+} (30 μM) in buffer solution from pH 1 to pH 13; Figure S9. Energy-optimized structure of **HDHT**–Cu^{2+} complex; Figure S10. (a) The theoretical excitation energies and the experimental UV–Vis spectrum of **HDHT**. (b) The major electronic-transition energies and molecular orbital contributions for **HDHT** (H = HOMO and L = LUMO); Figure S11. Molecular-orbital diagrams and excitation energies of **HDHT** and **HDHT**–Cu^{2+}; Figure S12. (a) The theoretical excitation energies and the experimental UV–Vis spectrum of **HDHT**–Cu^{2+}. (b) The major electronic transition energies and molecular-orbital contributions for **HDHT**–Cu^{2+} (H = HOMO and L = LUMO); Figure S13. Negative-ion ESI-MS spectra of **HDHT**–Cu^{2+} (100 μM) with S^{2-} (100 μM); Figure S14. The pH-stability test. (a) UV–Vis absorbance at 430 nm of **HDHT**–Cu^{2+} (30 μM) and **HDHT**–Cu^{2+} + S^{2-} (30 μM) in buffer solution from pH 1 to pH 13. (b) Color changes of **HDHT**–Cu^{2+} (30 μM) and **HDHT**–Cu^{2+} + S^{2-} (30 μM) in buffer solution from pH 1 to pH 13.

Author Contributions: H.N., S.M. and C.K. provided the initial idea for this work; H.N. contributed to the collection and analysis of the field-test data; H.N. and D.G. revised the paper; H.N., S.M. and C.K. wrote the paper. All authors have read and agreed to the published version of the manuscript.

Funding: This research was funded by the National Research Foundation of Korea, grant number 2020R1A6A1A0304274211.

Institutional Review Board Statement: Not applicable.

Informed Consent Statement: Not applicable.

Data Availability Statement: Not applicable.

Conflicts of Interest: The authors declare no conflict of interest.

References

1. Choe, D.; Kim, C. A Benzothiadiazole-Based Colorimetric Chemosensor for Detecting Cu^{2+} and Sequential H_2S in Practical Samples. *Inorg. Chim. Acta* **2022**, *543*, 121180. [CrossRef]
2. He, L.; Tao, H.; Koo, S.; Chen, G.; Sharma, A.; Chen, Y.; Lim, I.T.; Cao, Q.Y.; Kim, J.S. Multifunctional Fluorescent Nanoprobe for Sequential Detections of Hg^{2+} Ions and Biothiols in Live Cells. *ACS Appl. Bio Mater.* **2018**, *1*, 871–878. [CrossRef] [PubMed]
3. Sahu, M.; Manna, A.K.; Patra, G.K. A Fluorescent Colorimetric Vanillin Di-Schiff Base Chemosensor for Detection of Cu(II) and Isolation of Trinuclear Cu(II)-Dihydrazide. *Mater. Adv.* **2022**, *3*, 2495–2504. [CrossRef]
4. Asadpour Chounechenan, S.; Mohammadi, A.; Ghafouri, H. A New and Efficient Diaminopyrimidine-Based Colorimetric and Fluorescence Chemosensor for the Highly Selective and Sensitive Detection of Cu^{2+} in Aqueous Media and Living Cells. *Spectrochim. Acta A Mol. Biomol. Spectrosc.* **2022**, *267*, 120507. [CrossRef]
5. Kavitha, B.S.; Sridevi, S.; Makam, P.; Ghosh, D.; Govindaraju, T.; Asokan, S.; Sood, A.K. Highly Sensitive and Rapid Detection of Mercury in Water Using Functionalized Etched Fiber Bragg Grating Sensors. *Sens. Actuators B Chem.* **2021**, *333*, 129550.
6. Guan, W.L.; Zhang, Y.F.; Zhang, Q.P.; Zhang, Y.M.; Wei, T.B.; Yao, H.; Lin, Q. A Novel Fluorescent Chemosensor Based on Naphthofuran Functionalized Naphthalimide for Highly Selective and Sensitive Detecting Hg^{2+} and CN^{-}. *J. Lumin.* **2022**, *244*, 118722. [CrossRef]
7. Abebe, F.; Gonzalez, J.; Makins-Dennis, K.; Shaw, R. A New Bis(Rhodamine)-Based Colorimetric Chemosensor for Cu^{2+}. *Inorg. Chem. Commun.* **2020**, *120*, 108154. [CrossRef]
8. Aysha, T.S.; Mohamed, M.B.I.; El-Sedik, M.S.; Youssef, Y.A. Multi-Functional Colorimetric Chemosensor for Naked Eye Recognition of Cu^{2+}, Zn^{2+} and Co^{2+} Using New Hybrid Azo-Pyrazole/Pyrrolinone Ester Hydrazone Dye. *Dyes Pigm.* **2021**, *196*, 109795. [CrossRef]
9. Tavallali, H.; Deilamy-Rad, G.; Karimi, M.A.; Rahimy, E. A Novel Dye-Based Colorimetric Chemosensors for Sequential Detection of Cu^{2+} and Cysteine in Aqueous Solution. *Anal. Biochem.* **2019**, *583*, 113376. [CrossRef] [PubMed]
10. Zhao, M.; Zhang, Y.; Zheng, X.; Li, Z.; Xu, S. High Selective and Sensitive Optical Probe with Effective Recognition for Cu^{2+} Based on a Novel Aniline Squarylium Dye. *Inorg. Chem. Commun.* **2020**, *121*, 108198. [CrossRef]
11. Hu, Z.F.; Dou, L.; Zhang, J.; Zhang, Y.; Sun, Y.X.; Dong, W.K. A Novel "on-off-on" Halogen-Substituted Bis(Salamo)-like Fluorogenic Chemosensor for Sequentially Identifying Cu^{2+} Ions and Cysteine. *Inorg. Chim. Acta* **2022**, *541*, 121090. [CrossRef]
12. Ko, Y.G.; Mayank; Singh, N.; Jang, D.O. Single Chemosensor for Sensing Multiple Analytes: Selective Fluorogenic Detection of Cu^{2+} and Br^{-}. *Tetrahedron Lett.* **2018**, *59*, 3839–3844. [CrossRef]
13. Pungut, N.A.S.; Heng, M.P.; Saad, H.M.; Sim, K.S.; Lee, V.S.; Tan, K.W. From One to Three, Modifications of Sensing Behavior with Solvent System: DFT Calculations and Real-Life Application in Detection of Multianalytes (Cu^{2+}, Ni^{2+} and Co^{2+}) Based on a Colorimetric Schiff Base Probe. *J. Mol. Struct.* **2021**, *1238*, 130453. [CrossRef]
14. Lee, J.C.; Gray, H.B.; Winkler, J.R. Copper (II) Binding to Alpha-Synuclein, the Parkinson' s Protein. *J. Am. Chem. Soc.* **2008**, *130*, 6898–6899. [CrossRef]
15. Kim, B.E.; Nevitt, T.; Thiele, D.J. Mechanisms for Copper Acquisition, Distribution and Regulation. *Nat. Chem. Biol.* **2008**, *4*, 176–185. [CrossRef]
16. Kshtriya, V.; Koshti, B.; Pandey, D.K.; Kharbanda, S.; Chandra Kanth, P.; Singh, D.K.; Bhatia, D.; Gour, N. Sequential and Cellular Detection of Copper and Lactic Acid by Disaggregation and Reaggregation of the Fluorescent Panchromatic Fibres of an Acylthiourea Based Sensor. *Soft Matter* **2021**, *17*, 4304–4316. [CrossRef]
17. Kim, A.; Kang, J.H.; Jang, H.J.; Kim, C. Fluorescent Detection of Zn(II) and In(III) and Colorimetric Detection of Cu(II) and Co(II) by a Versatile Chemosensor. *J. Ind. Eng. Chem.* **2018**, *65*, 290–299. [CrossRef]
18. Cheah, P.W.; Heng, M.P.; Saad, H.M.; Sim, K.S.; Tan, K.W. Specific Detection of Cu^{2+} by a PH-Independent Colorimetric Rhodamine Based Chemosensor. *Opt. Mater.* **2021**, *114*, 110990. [CrossRef]
19. Mohanasundaram, D.; Bhaskar, R.; Sankarganesh, M.; Nehru, K.; Gangatharan Vinoth Kumar, G.; Rajesh, J. A Simple Pyridine Based Fluorescent Chemosensor for Selective Detection of Copper Ion. *Spectrochim. Acta A Mol. Biomol. Spectrosc.* **2022**, *265*, 120395. [CrossRef]
20. Ozmen, P.; Demir, Z.; Karagoz, B. An Easy Way to Prepare Reusable Rhodamine-Based Chemosensor for Selective Detection of Cu^{2+} and Hg^{2+} Ions. *Eur. Polym. J.* **2022**, *162*, 110922. [CrossRef]
21. Rajasekaran, D.; Venkatachalam, K.; Periasamy, V. "On–off–on" Pyrene-Based Fluorescent Chemosensor for the Selective Recognition of Cu^{2+} and S^{2-} Ions and Its Utilization in Live Cell Imaging. *Appl. Organomet. Chem.* **2020**, *34*, e5342. [CrossRef]
22. Feng, S.S.; Wei, Y.X.; Li, M.; Dong, W.K. A Highly Selective Naphthalene-Fluorophore Salamo-Based Chemosensor for Sequential Identification of Cu^{2+} and S^{2-} Ions in Water Applications. *J. Mol. Struct.* **2022**, *1261*, 132923. [CrossRef]
23. Pan, Y.Q.; Xu, X.; Zhang, Y.; Zhang, Y.; Dong, W.K. A Highly Sensitive and Selective Bis(Salamo)-Type Fluorescent Chemosensor for Identification of Cu^{2+} and the Continuous Recognition of S^{2-}, Arginine and Lysine. *Spectrochim. Acta A Mol. Biomol. Spectrosc.* **2020**, *229*, 117927. [CrossRef] [PubMed]

24. Mu, H.R.; Yu, M.; Wang, L.; Zhang, Y.; Ding, Y.J. Catching S^{2-} and Cu^{2+} by a Highly Sensitive and Efficient Salamo-like Fluorescence-Ultraviolet Dual Channel Chemosensor. *Phosphorus Sulfur Silicon Relat. Elem.* **2020**, *195*, 730–739. [CrossRef]
25. Kargar, M.; Darabi, H.R.; Sharifi, A.; Mostashari, A. A New Chromogenic and Fluorescent Chemosensor Based on a Naphthol-Bisthiazolopyridine Hybrid: A Fast Response and Selective Detection of Multiple Targets, Silver, Cyanide, Sulfide, and Hydrogen Sulfide Ions and Gaseous H_2S. *Analyst* **2020**, *145*, 2319–2330. [CrossRef]
26. Jung, J.M.; Kang, J.H.; Han, J.; Lee, H.; Lim, M.H.; Kim, K.T.; Kim, C. A Novel "off-on" Type Fluorescent Chemosensor for Detection of Zn^{2+} and Its Zinc Complex for "on-off" Fluorescent Sensing of Sulfide in Aqueous Solution, in Vitro and in Vivo. *Sens. Actuators B Chem.* **2018**, *267*, 58–69. [CrossRef]
27. Wang, P.; Zhou, D.; Xue, S.; Chen, B.; Wen, S.; Yang, X.; Wu, J. Rational Design of Dual-Functional Peptide-Based Chemosensor for Sequential Detection of Ag^{+} (AgNPs) and S^{2-} Ions by Fluorescent and Colorimetric Changes and Its Application in Live Cells, Real Water Samples and Test Strips. *Microchem. J.* **2022**, *177*, 107326. [CrossRef]
28. Chen, F.; Han, D.; Liu, H.; Wang, S.; Li, K.B.; Zhang, S.; Shi, W. A Tri-Site Fluorescent Probe for Simultaneous Sensing of Hydrogen Sulfide and Glutathione and Its Bioimaging Applications. *Analyst* **2018**, *143*, 440–448. [CrossRef]
29. Thai, D.A.; Lee, N.Y. A Paper-Based Colorimetric Chemosensor for Rapid and Highly Sensitive Detection of Sulfide for Environmental Monitoring. *Anal. Methods* **2021**, *13*, 1332–1339. [CrossRef]
30. Kim, M.S.; Jung, J.M.; Ahn, H.M.; Kim, C. A Simple Colorimetric Chemosensor for Relay Detection of Cu^{2+} and S^{2-} in Aqueous Solution. *J. Coord. Chem.* **2018**, *71*, 355–370. [CrossRef]
31. Singh, N.; Chandra, R. A Naked-Eye Colorimetric Sensor Based on Chalcone for the Sequential Recognition of Copper(II) and Sulfide Ions in Semi-Aqueous Solution: Spectroscopic and Theoretical Approaches. *New J. Chem.* **2021**, *45*, 10340–10348. [CrossRef]
32. Wang, P.; Sun, L.; Wu, J.; Yang, X.; Lin, P.; Wang, M. A Dual-Functional Colorimetric and Fluorescent Peptide-Based Probe for Sequential Detection of Cu^{2+} and S^{2-} in 100% Aqueous Buffered Solutions and Living Cells. *J. Hazard. Mater.* **2021**, *407*, 124388. [CrossRef] [PubMed]
33. Sun, T.; Niu, Q.; Li, T.; Guo, Z.; Liu, H. A Simple, Reversible, Colorimetric and Water-Soluble Fluorescent Chemosensor for the Naked-Eye Detection of Cu^{2+} in ~ 100% Aqueous Media and Application to Real Samples. *Spectrochim. Acta A Mol. Biomol. Spectrosc.* **2018**, *188*, 411–417. [CrossRef] [PubMed]
34. Park, S.; Choe, D.; Lee, J.J.; Kim, C. A Benzyl Carbazate-Based Colorimetric Chemosensor for Relay Detection of Cu^{2+} and S^{2-} in near-Perfect Aqueous Media. *J. Mol. Struct.* **2021**, *1240*, 130576. [CrossRef]
35. So, H.; Chae, J.B.; Kim, C. A Thiol-Containing Colorimetric Chemosensor for Relay Recognition of Cu^{2+} and S^{2-} in Aqueous Media with a Low Detection Limit. *Inorg. Chim. Acta* **2019**, *492*, 83–90. [CrossRef]
36. Parua, S.P.; Sinha, D.; Rajak, K.K. A Highly Selective "on-off-on" Optical Switch for Sequential Detection of Cu^{2+} and S^{2-} Ions Based on 2, 6-Diformyl-4-Methyl Phenol and Catecholase Activity by Its Copper Complex. *ChemistrySelect* **2018**, *3*, 1120–1128. [CrossRef]
37. Jin, X.; Chen, H.; Zhang, W.; Wang, B.; Shen, W.; Lu, H. A Novel Purine Derivative-Based Colorimetric Chemosensor for Sequential Detection of Copper Ion and Sulfide Anion. *Appl. Organomet. Chem.* **2018**, *32*, e4577. [CrossRef]
38. Kwon, N.; Chen, Y.; Chen, X.; Kim, M.H.; Yoon, J. Recent Progress on Small Molecule-Based Fluorescent Imaging Probes for Hypochlorous Acid (HOCl)/Hypochlorite (OCl^{-}). *Dyes Pigm.* **2022**, *200*, 110132. [CrossRef]
39. Lee, S.; Jen, M.; Jang, T.; Lee, G.; Pang, Y. Twisted Intramolecular Charge Transfer of Nitroaromatic Push–Pull Chromophores. *Sci. Rep.* **2022**, *12*, 6557. [CrossRef]
40. Kajetanowicz, A.; Grela, K. Nitro and Other Electron Withdrawing Group Activated Ruthenium Catalysts for Olefin Metathesis Reactions. *Angew. Chemie Int. Ed.* **2021**, *60*, 13738–13756. [CrossRef]
41. Vojinović-Ješić, L.S.; Češljević, V.I.; Bogdanović, G.A.; Leovac, V.M.; Szécsényi, K.M.; Divjaković, V.; Joksović, M.D. Transition Metal Complexes with Girard Reagent-Based Ligands. Part V. Synthesis, Characterization and Crystal Structure of Pentagonal-Bipyramidal Manganese(II) Complex with 2,6-Diacetylpyridine Bis(Girard-T Hydrazone). *Inorg. Chem. Commun.* **2010**, *13*, 1085–1088. [CrossRef]
42. Moussa, M.N.H.; El-Far, A.A.; El-Shafei, A.A. The Use of Water-Soluble Hydrazones as Inhibitors for the Corrosion of C-Steel in Acidic Medium. *Mater. Chem. Phys.* **2007**, *105*, 105–113. [CrossRef]
43. Bogdanov, A.V.; Zaripova, I.F.; Voloshina, A.D.; Sapunova, A.S.; Kulik, N.V.; Voronina, J.K.; Mironov, V.F. Synthesis and Antimicrobial Study of Novel 1-Benzylated Water-Soluble Isatin-3-Hydrazones. *Chem. Biodivers.* **2018**, *15*, 1800088. [CrossRef] [PubMed]
44. Frisch, M.J.; Trucks, G.W.; Schlegel, H.B.; Scuseria, G.E.; Robb, M.A.; Cheeseman, J.R.; Scalmani, G.; Barone, V.; Petersson, G.A.; Nakatsuji, H.; et al. *Gaussian 16 Revision C.01*; Gaussian, Inc.: Walingford, CT, USA, 2016.
45. Becke, A.D. Density-functional Thermochemistry. III. The Role of Exact Exchange. *J. Chem. Phys.* **1993**, *98*, 5648–5652. [CrossRef]
46. Lee, C.; Yang, W.; Parr, R.G. Development of the Colle-Salvetti Correlation-Energy Formula into a Functional of the Electron Density. *Phys. Rev. B* **1988**, *37*, 785–789. [CrossRef] [PubMed]
47. Hariharan, P.C.; Pople, J.A. The Influence of Polarization Functions on Molecular Orbital Hydrogenation Energies. *Theor. Chim. Acta* **1973**, *28*, 213–222. [CrossRef]
48. Francl, M.M.; Pietro, W.J.; Hehre, W.J.; Binkley, J.S.; Gordon, M.S.; DeFrees, D.J.; Pople, J.A. Self-consistent Molecular Orbital Methods. XXIII. A Polarization-type Basis Set for Second-row Elements. *J. Chem. Phys.* **1982**, *77*, 3654–3665. [CrossRef]

49. Wadt, W.R.; Hay, P.J. Ab Initio Effective Core Potentials for Molecular Calculations. Potentials for Main Group Elements Na to Bi. *J. Chem. Phys.* **1985**, *82*, 284–298. [CrossRef]
50. Klamt, A.; Moya, C.; Palomar, J. A Comprehensive Comparison of the IEFPCM and SS(V)PE Continuum Solvation Methods with the COSMO Approach. *J. Chem. Theory Comput.* **2015**, *11*, 4220–4225. [CrossRef]
51. Ershov, A.Y.; Lagoda, I.V.; Yakimovich, S.I.; Pakal'Nis, V.V.; Zerova, I.V.; Dobrodumov, A.V.; Shamanin, V.V. Tautomerism and Conformational Isomerism of Mercaptoacetylhydrazones of Aliphatic and Aromatic Aldehydes. *Russ. J. Org. Chem.* **2009**, *45*, 660–666. [CrossRef]
52. Gil, D.; Lee, J.J.; Lee, H.; Kim, K.-T.; Kim, C. Detection of Environmentally Hazardous Hypochlorite in Pure Water with a Novel Fluorescent Chemosensor: Application to Water Samples, Commercial Disinfectants, Test Strips, and Zebrafish. *Dyes Pigm.* **2022**, *207*, 110714. [CrossRef]
53. Mahnashi, M.H.; Mahmoud, A.M.; Alkahtani, S.A.; Ali, R.; El-Wekil, M.M. A Novel Imidazole Derived Colorimetric and Fluorometric Chemosensor for Bifunctional Detection of Copper (II) and Sulphide Ions in Environmental Water Samples. *Spectrochim. Acta A Mol. Biomol. Spectrosc.* **2020**, *228*, 117846. [CrossRef]
54. Rajendra Prasad, Y.; Kumar, P.P.; Kumar, P.R.; Rao, A.S. Synthesis and Antimicrobial Activity of Some New Chalcones of 2-Acetyl Pyridine. *J. Chem.* **2008**, *5*, 144–148.
55. Rout, K.C.; Mondal, B. Copper(II) Complex as Selective Turn-on Fluorescent Probe for Nitrite Ion. *Inorg. Chim. Acta* **2015**, *437*, 54–58. [CrossRef]
56. Nouri Moghadam, F.; Amirnasr, M.; Meghdadi, S.; Eskandari, K.; Buchholz, A.; Plass, W. A New Fluorene Derived Schiff-Base as a Dual Selective Fluorescent Probe for Cu^{2+} and CN^{-}. *Spectrochim. Acta A Mol. Biomol. Spectrosc.* **2019**, *207*, 6–15. [CrossRef]
57. Rha, C.J.; Lee, H.; Kim, C. An Effective Phthalazine-Imidazole-Based Chemosensor for Detecting Cu^{2+}, Co^{2+} and S^{2-} via the Color Change. *Inorg. Chim. Acta* **2020**, *511*, 119788. [CrossRef]